Annex II

Modelling polymer-based Love-mode transducers acting as gravimetric sensors

J.-M Friedt[1], S. Alzuaga[2], T. Baron[2], W. Daniau [2], S. Ballandras[2]
[1] SENSeOR, Besançon, France
[2] FEMTO-ST Time & Frequency, Besançon, France
May 13, 2013

1 Introduction

The physical quantities under investigation are the acoustic wave velocity and losses. The most basic approach to velocity measurement is a time of flight measurement, or its implementation in terms of continuous wave with a phase measurement between the input signal and the output signal propagating through the acoustic device sensing area.

2 Free space acoustic velocity and mass sensitivity

The first modelling step aims at identifying the free space propagation loss and coupling coefficients in order to obtain a rough estimate of the working conditions of the device. The velocity dependence with the guiding layer thickness also provides an estimate of the gravimetric sensitivity following considerations similar to establishing the Sauerbrey relation in which the boundary condition is slightly modified to assess the sensitivity. While in a bulk acoustic resonator the relationship between substrate thickness and operating frequency is obvious by differentiating $f = c/\lambda$, the velocity v.s guiding layer thickness in the case of the guided Love mode is not obvious and requires dedicated modelling tools.

The basic input of modelling the guiding layer requires the mechanical and electrical material constants. From the well known relationships [1], the tabulated Young modulus E and Poisson coefficient ν are used to generate the constants for an isotropic material

$$c_{11} = \frac{E(1-\nu)}{(1+\nu)(1-2\nu)} \qquad c_{12} = \frac{E\nu}{(1+\nu)(1-2\nu)}$$

and

$$c_{11} = c_{22} = c_{33} \qquad c_{44} = c_{55} = c_{66} = \frac{c_{11} - c_{12}}{2} \qquad c_{12} = c_{13} = c_{23}$$

While rather well known for common materials such as silicon dioxide, these constants exhibits significant dispersion for polymers. Based on the values provided by the Goodfellow catalog for PMMA, the constant file was generated and used to model the free space propagation velocity and coupling over AT and ST quartz substrates as a function of guiding layer thickness (Fig. 1).

Propagation characteristics of the guided wave are strongly dependent on the guiding material characteristics. For validation of the modelling procedure, PMMA was replaced with the more familiar SiO_2, which indeed exhibits a much slower velocity decrease with increasing guiding layer thickness due to the lower mismatch of the quartz to guiding layer velocities.

The gravimetric sensitivity S defining the relative frequency shift $\Delta f/f$ when submitting an acoustic device to a mass loading of ΔM over its sensing area A is given by

$$S = \frac{\Delta f}{f} \times \frac{A}{\Delta M}$$

in cm^2/g units. The larger the sensitivity, the larger the relative frequency shift for a given mass loading. Since the deposited mass of a material of density ρ is also given when coating a thickness Δt by $\Delta M = \rho A \Delta t$, the gravimetric sensitivity is also expressed as $\frac{\Delta f}{f} \times \frac{1}{\rho \Delta t}$. Since the acoustic velocity v and frequency f are related by the wavelength λ which is kept constant (as defined by the interdigitated electrode spacing), we obtain $\frac{\Delta f}{f} = \frac{\Delta v}{v}$ and we conclude from Fig. 1 that since the derivate of the velocity with guiding layer thickness is much steeper for PMMA than for SiO_2, the gravimetric sensitivity is expected to be also increased.

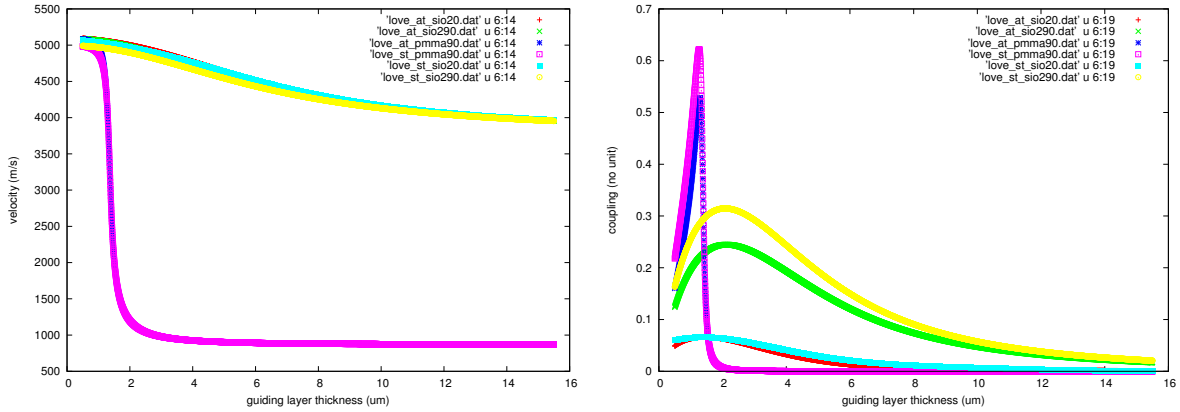

Figure 1: Propagation characteristics of a Love mode guided acoustic wave as a function of guiding layer thicknesses, for PMMA and silicon dioxide coating over ST-cut quartz. Left the velocity, right the coupling.

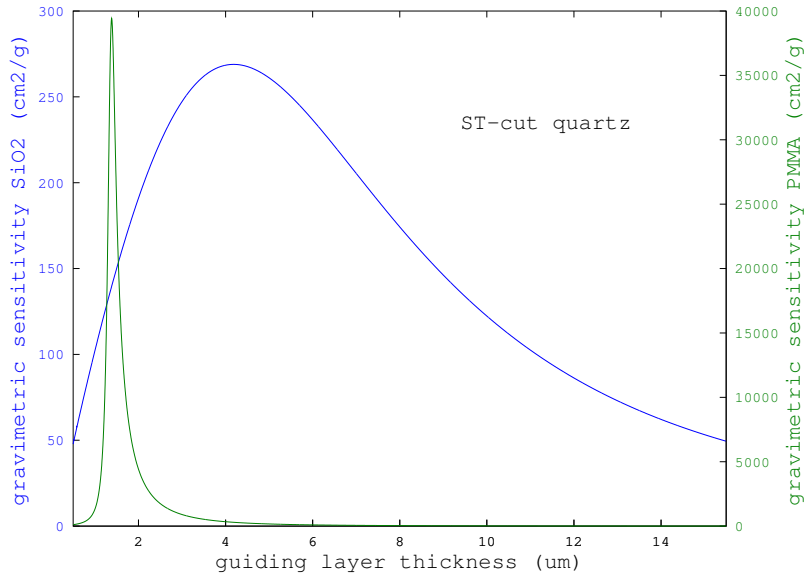

Figure 2: Gravimetric sensitivity of the silicon dioxide coated and PMMA coated ST-cut quartz transducer. Although the gravimetric sensitivity of the silicon dioxide device is reasonable and consistent with experiment [2], the PMMA guided device sensitivity seems excessively optimistic.

The unrealistic gravimetric sensitivity found through the normalized derivate of the velocity when guiding the acoustic wave in PMMA is attributed to the material constants which should be adapted to yield more reasonable sensitivity values. Nevertheless, this simulation seems to indicate that much thinner PMMA guiding layers should be used than those used for silicon dioxide coated devices, and most significantly appears consistent with the literature [3] in which a gravimetric sensitivity as high as 6700 cm^2/g seems to be presented [1]. The sharp loss of coupling and narrow range of acceptable guiding layer thicknesses will have strong consequences in the following modelling steps. So far all these simulations were performed with viscous water loading on the sensor: however, due to the difficult algorithm convergence when searching for acoustic wave propagation parameters, the following steps will

[1] Fig 3(a) of [3] hints at a velocity variation from 4700 to 2500 m/s when the guiding layer thickness increases from $k \times \lambda$ values from 0.5 to 0.7, or 1 μm thickness increase at $\lambda = 30$ μm

be performed without viscoelastic loading in order to reduce acoustic loss contributions and improve the capability of identifying an acoustic mode.

Notice that the wireless sensing mechanism described earlier also provides some capability of measurement in liquid phase through a wireless sensing strategy [4, 5].

3 Acoustic velocity over an infinite periodic grating

As a rough approximation, a resonator is a sequence of areas patterned with periodic metallic grating, whether in the Bragg mirror (floating potential transducers spaced by the coherent energy accumulation conditions) region, the transducer made of interdigitated transducer patterns, or the acoustic cavity which might or might not be structured with a periodic pattern. The acoustic properties of each region is well modelled by assuming that the periodic pattern geometrical features are repeated infinitely. This assumption, completed with radiating boundary conditions implemented as Green functions, is the basics of the modelling tools available at the FEMTO-ST time & frequency laboratory.

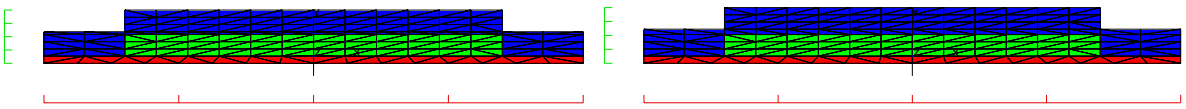

Figure 3: Finite element model mesh when simulating a single electrode. Notice how the guiding layer is assumed to follow the patterned substrate topography. The guiding layer thickness was increased between the left and right models.

The degrees of freedom of the model are:

1. substrate orientation
2. electrode thickness,
3. electrode width to period ratio
4. guiding layer thickness

Sweeping these parameters, a matrix of the most significant design parameters including acoustic velocity, reflection coefficient, beam steering, conductance, static capacitance and permittivity is extracted. This very rich set of information is processed to combine the most appropriate mechanical properties (metallic layer thickness, electrode width and period, guiding layer thickness) of the various regions. As opposed to the basic transmission delay line in which each electrode only acts as an electric field generator, the mechanical properties (reflection due to the impedance mismatch associated with electrode mass loading) are also used in designing a resonator.

Among the simulation challenges, the Love wave exhibits a very strong sensitivity with the guiding layer thickness, which is actually maximized since it is representative of the gravimetric sensitivity of the device. Thus, the simulation software cannot be operated in a single frequency range but a tracking of the mode must be implemented to closely follow the position of the region of interest. Furthermore, the fitting procedure needed to extract the propagation parameters never converges for PMMA thicknesses

above 5% of the wavelength, which thus restricts the analysis to the sub-1.5 μm range (Fig. 4), or the initial velocity (and free space coupling) drop.

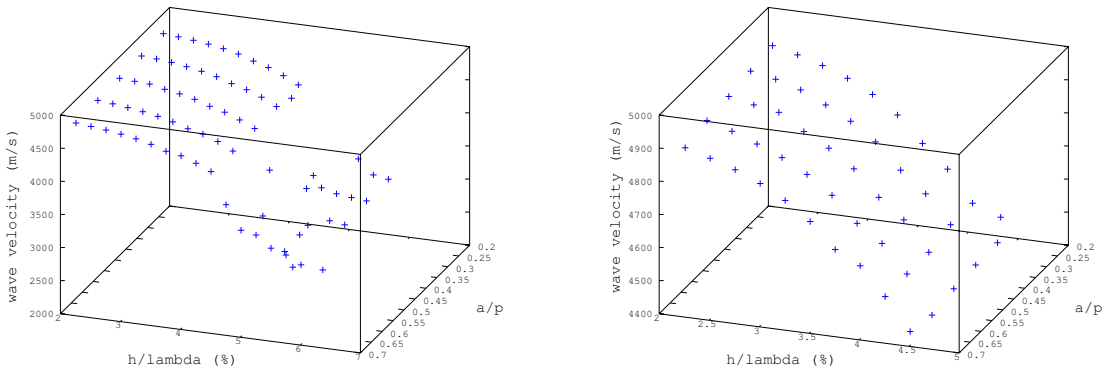

Figure 4: Propagation velocity of the Love mode acoustic wave: the aluminum thickness is kept constant throughout the simulations and only the PMMA guiding layer thickness is varied (h/λ parameter). The other parameter is the metalization ratio. Left: the whole explored parameter space, with PMMA thicknesses up to 7% of the wavelength (2.1 μm at λ=30 μm). Right: zoom on the parameter range for which the wave propagation characteristics were properly extracted.

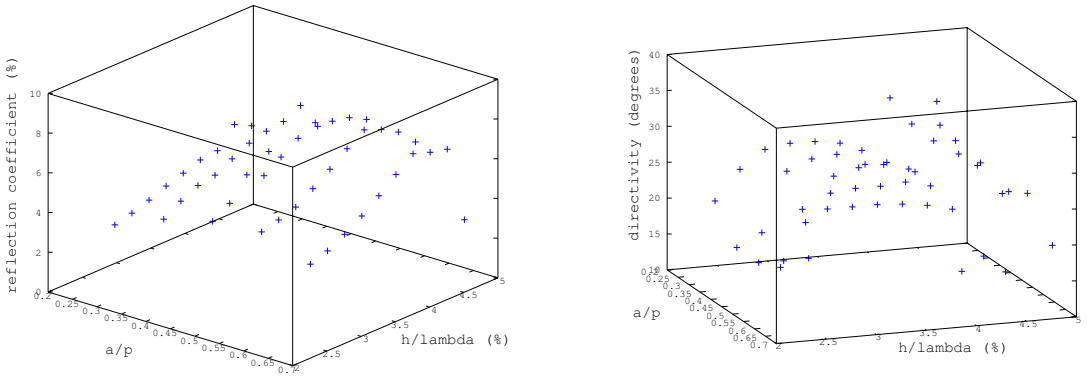

Figure 5: Reflection coefficient (left) and directivity (right) of the Love mode acoustic propagation over an infinite periodic grating. The display is restricted to the parameter range for which the wave propagation characteristics were properly extracted.

All propagation parameters presented here were processed for a fixed aluminum metalization thickness of 2% of the wavelength, or 600 nm. This parameter was varied from 0 up to the PMMA thickness during the simulations but was found to hardly affect the propagation parameters which were most significantly affected by the PMMA thickness.

Having extracted the propagation characteristics over infinite gratings, the practical acoustic device made of a finite number of electrodes is modelled using a mixed matrix approach in which the propagation characteristics of each individual cell – as extracted from the propagation parameter matrices we just described – are cascaded to access to the transfer function of the whole device.

4 Acoustic velocity over a finite periodic grating: resonator

4.1 Delay line configuration

Before tackling the issue of resonator modelling, we wish to assess whether the generated propagation parameters are representative of the current delay line design already used. A 4-electrode in each electrical period design is used in order to prevent the interdigitated transducers from acting as reflectors.

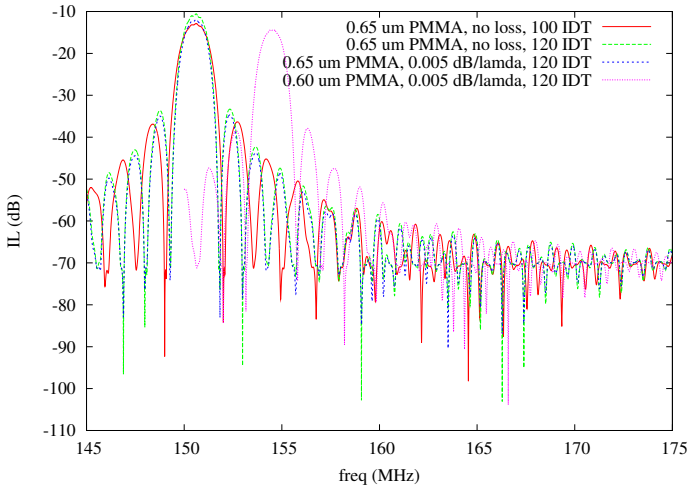

Figure 6: Modelled Transfer function of a transmission delay line operating with a λ=30 μm wavelength. Various guiding layer thicknesses are considered to assess the gravimetric sensitivity, as well as the propagation losses in the guiding layer.

Varying the PMMA layer thickness of the guiding layer simulates the adsorption of a layer on the sensing surface (which justifies the perturbative approach, as proposed by Sauerbrey, of varying the boundary condition to assess the gravimetric sensitivity of the transducer). Fig. 6 exhibits on the one hand the influence of a loss-less and lossy (0.005 dB/λ) guiding layer, and varying the guiding layer thickness to extract an estimate of the gravimetric sensitivity. The former comparison demonstrates, as expected from a poorly coupled material as quartz, that the insertion loss level is driven by the coupling coefficient of the piezoelectric substrate rather than the propagation losses. The latter comparison yields the following estimate of the gravimetric sensitivity: a Δe =50 nm PMMA thickness variation yields a frequency of the maximum of the transfer function shift by about 4 MHz, hence a sensitivity $S = \frac{\Delta f}{f} \times \frac{1}{\rho \Delta e} = \frac{4}{152} \times \frac{1}{1.19 \times 50.10^{-7}} \simeq 4400$ cm^2/g. This value is consistent, although as unreasonable, as the one found initially in a free space propagation simulation. Experimental transfer function indeed match the modelled responses (Fig. 7).

4.2 Resonator configuration: 5000 μm long cavity

The first simulation is performed on a resonator with random cavity length, selected at the same size than the one used for the delay line, namely 5000 μm which is not an integer number of periods (as a reminder, $\lambda = 30$ μm).

A resonator is made of three elements: a cavity, a set of interdigitated transducers (IDTs) and mirrors for confining the energy within the cavity. The cavity might be free of electrode or might be patterned IDTs, meeting a continuity characteristics with the transducer characteristics (synchronous configuration) or with characteristics mismatch (asynchronous configuration [6]).

The number of IDTs in the transducer and mirror defines the transfer function and quality factor. The cavity dimension is defined by the user: in our case it must be long enough to allow for easy positioning of the fluidic cell. Although cavities are classically in the few wavelength long, the required 5 mm gap will be in our case more than 150 wavelengths long. Since acoustic losses in the gap are not accounted

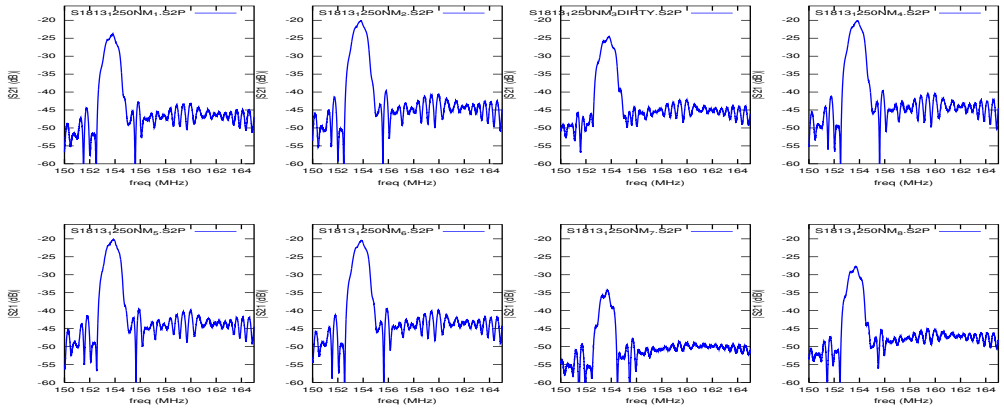

Figure 7: Experimental transfer functions of 155 MHz delay lines manufactured at the MIMENTO facility of FEMTO-ST. A 1.25 μm thick S1813 photoresist coating acts as a guiding layer for the Love wave. Typical insertion losses are in the -20 dB range.

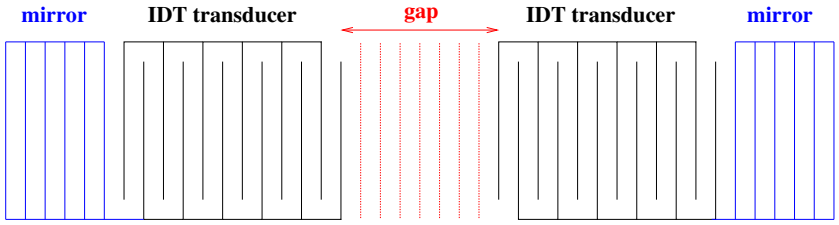

Figure 8: The three main parts of a resonator are the sensing area made of a gap between the interdigitated transducer. The acoustic energy confinement is brought by the two Bragg mirrors surrounding the sensing area. The gap might or might not be patterned with a periodic structure.

for, the only consequence of varying the gap (cavity) length is to change the number of acoustic modes confined in the cavity.

One particular issue is the propagation parameter in the cavity free of electrodes: the acoustic velocity must be provided as found in the initial simulation (section 2)

From these preliminary results (Figs. 10, 11, 12 with a sensing cavity gap 5000 μm long, which is *not* an integer number of periods), one sees that the reflection coefficient in the Bragg mirror is strong enough for the properties of the resonator to converge after only about 100 IDTs: all energy has been reflected and longer reflectors are no longer needed.

4.3 Resonator configuration: 5010 μm long cavity

In order to assess the sensitivity of the design to the cavity length, a new simulation was performed with a 5010 μm long cavity, or 167 wavelengths (Figs. 13,14).

No significant difference is observed with respect to the simulation on a 5000 μm-long cavity resonator, so it seems that for such large cavities the relative position of the IDT combs is not significant. Insertion losses are minimized for 150 electrodes in the mirror, or a total mirror length of both mirrors of 2×2250 μm or 4.5 mm of the total transducer length. Adding the 5 mm cavity and the 50 IDTs in the transducer (since the insertion loss seems mostly insensitive to IDT length), the total device length is estimated to be 12.5 mm. An aperture of 400 μm, matching the wide than 10λ condition, seems appropriate: all simulations are 2D and do not include the effect of busses.

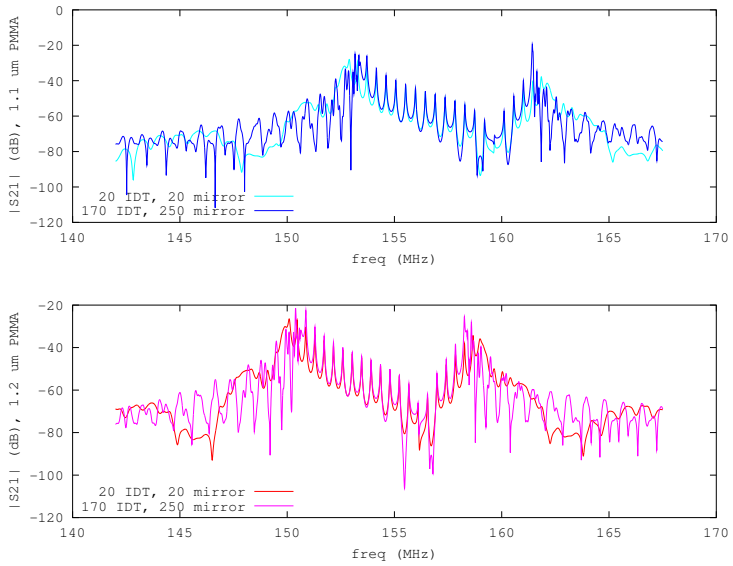

Figure 9: Typical spectra resulting from simulations in which the number of electrodes in the IDTs or in the mirror is varied, as well as the PMMA thickness. The metal thickness of the aluminum electrodes was kept constant throughout all the simulations at 600 nm.

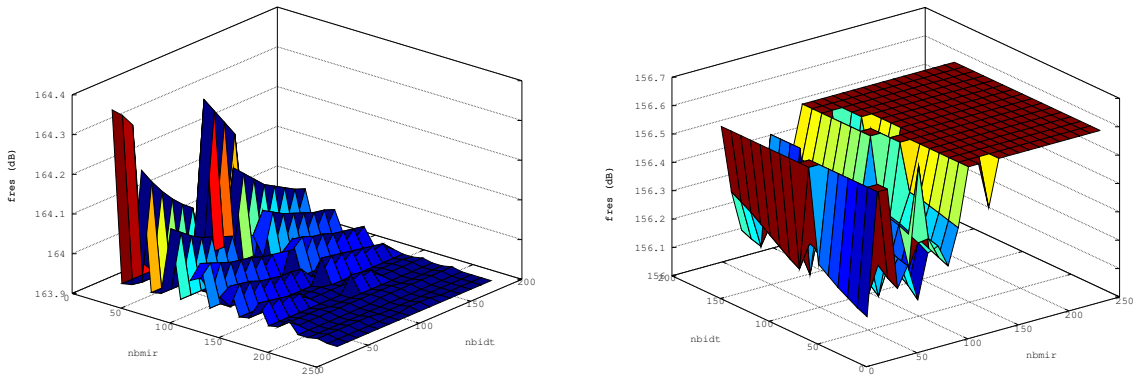

Figure 10: Evolution of the mode frequency at the input (right) and output (left) of the stop band. Notice that the horizontal axis has been rotated between the representation of the two curves.

4.4 Resonator configuration: 5010 μm long cavity filled with a grating

So far we have considered IDTs and Bragg mirrors surrounding a pattern free cavity. We now consider the case of filling the cavity with a periodic pattern of electrodes meeting continuity conditions with the transducer IDTs.

The modes within the stop band have now disappeared since they no longer meet confinement conditions as the cavity is filled with a periodic grating (Fig. 15. Cleaning these spurious modes might be relevant for oscillator applications but in an openloop approach in which the probed frequency is defined by the frequency synthesizer source, the improvement is not useful. The optimum insertion loss seems to be observed for about 100 grating periods in the mirror (Fig. 16).

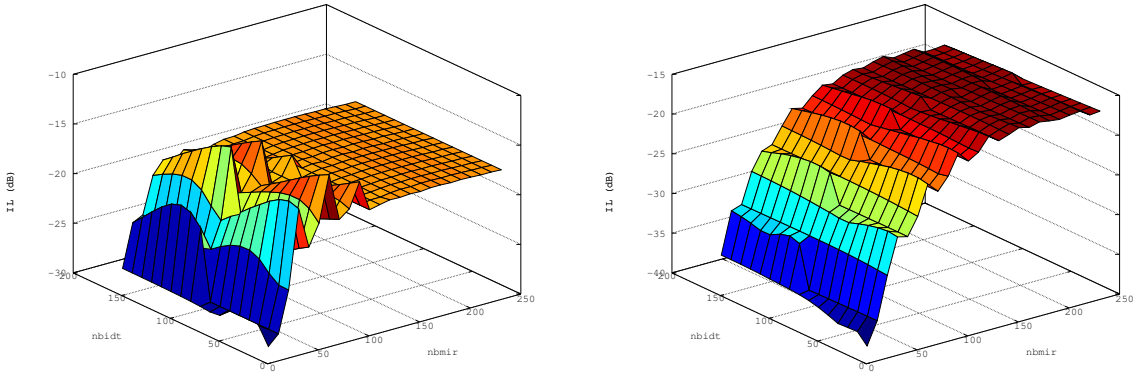

Figure 11: Evolution of the insertion losses of mode at the the input (right) and output (left) of the stop band.

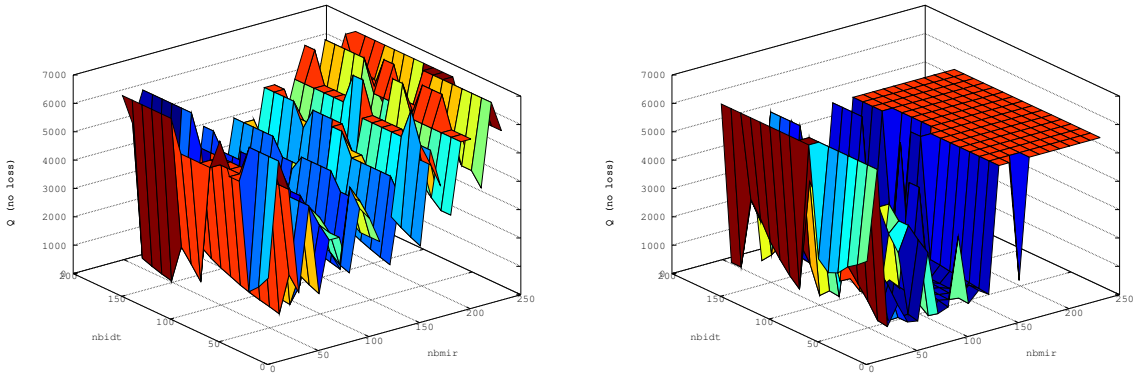

Figure 12: Evolution of the quality factor of mode at the the input (right) and output (left) of the stop band.

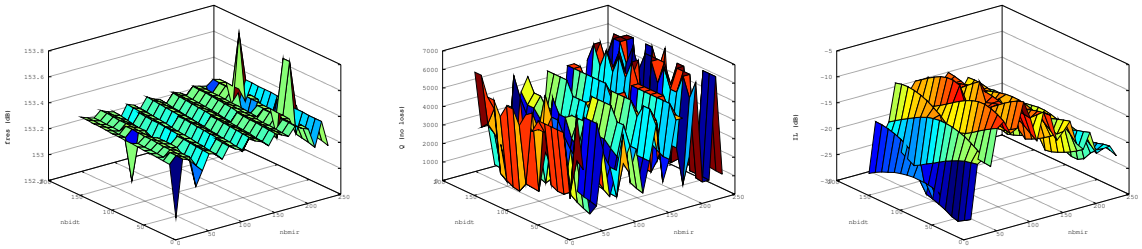

Figure 13: Evolution of the acoustic resonance parameter at the input of the stop band.

5 Gravimetric sensitivity

All simulation were performed with vacuum over the surface propagating the acoustic wave and thus not viscoelastic loss in the surrounding medium has been accounted for. Under the assumption of a purely gravimetric interaction, the sensitivity can be identified for each case described earlier by slightly varying the guiding layer thickness, simulating the adsorption of a layer on top of the surface propagating the shear acoustic wave (we have considered $\rho_{PMMA} = 1.185$ g.cm^{-3}). Both input of the stop-band mode (S_{in}) and output of the stop-band (S_{out}) are given. Previous experiments indicate that only one of these

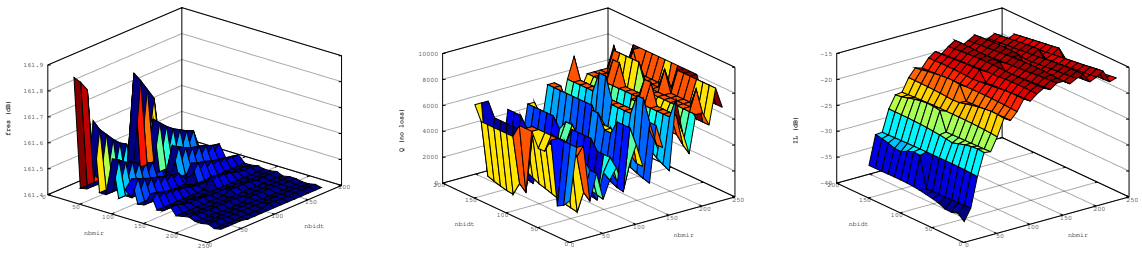

Figure 14: Evolution of the acoustic resonance parameter at the output of the stop band.

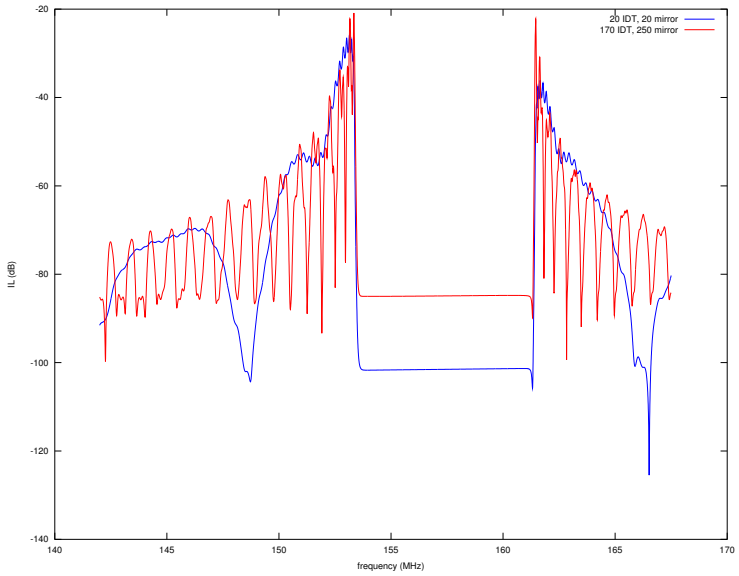

Figure 15: Typical spectra of the transducer whose cavity is filled with a grating.

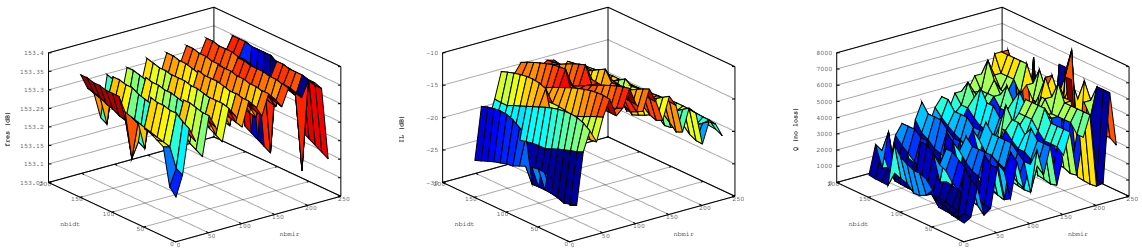

Figure 16: Evolution of the acoustic resonance parameter at the input of the stop band when the 5010 μm long cavity is filled with a periodic grating.

two modes will be robust to viscoelastic loading.

transducer	stop-band input freq. 1.1 μm PMMA (MHz)	stop-band input freq. 1.2 μm PMMA (MHz)	stop-band output freq. 1.1 μm PMMA (MHz)	stop-band output freq. 1.2 μm PMMA (MHz)	S_{in} cm^2/g	S_{out} cm^2/g
5000 μm free	153.324	150.731	161.481	158.540	1430	1540
5010 μm free	153.161	150.392	161.423	158.266	1530	1650
5010 μm grating	153.346	150.568	161.46	158.410	1530	1590

6 Experimental assessment

A mask has been designed which includes most of the modelling conditions stated in this report. IDTs are 50 or 100-finger pairs long, mirrors are 100 or 150 electrode long, and the cavity is either coated with a full metallic layer (acting as Faraday cage) or with a grating whose electrodes are either grounded or left floating. A total of 14 differential devices (Fig. 17) operating around 155 MHz (32 μm wavelength) fit on a 4 inch wafer. The first set of measurements were made of delay lines: the low acoustic losses observed when using the polymer guiding layer have already been discussed earlier (Fig. 7). One additional information gathered from these measurements by varying the guiding layer thickness is the gravimetric sensitivity of the device: an increase by 400 nm of the guiding layer thickness yields a shift in the transfer function maximum from 156.495 to 153.820 MHz, yielding a gravimetric sensitivity of **360 cm^2/g** if we assume the density of the resist to be 1.2 g/cm^3.

The first questionable assumption is the conformational shape of the polymer surface when coating the IDT patterned quartz surface. We have assumed in the model that the same topography is reproduced from the IDT patterned surface to the top of the photoresist coating. This surface structure significantly affects the modelled reflection coefficient and thus the quality factor for a given number of electrodes in the mirrors. We have experimentally observed that the surface topography structure depth is strongly diminished with respect to the aluminum electrode thickness, most probably due to surface tension on the fluid photoresist during curing. A summary of the observed surface topography is provided in Tab. 1

Al thickness (nm)	photoresist thickness (nm)	surface topography (nm)
445	1200	145
445	2600	30

Table 1: Surface topography as a function of polymer layer thickness. The assumption in the models of a transfer of the Al electrode topography to the polymer surface is questionable.

Nevertheless, all structures discussed in the simulation part were manufactured, including sensing cavities free of electrodes or patterned with a synchronous grating of electrodes. Various photoresist thicknesses were deposited to assess the gravimetric sensitivity. The temperature dependence of these devices was experimentally assessed in order to try and identify conditions which would reduce as much as possible temperature drift, even though the use of a better coupled ST-cut quartz substrate is known never exhibit temperature compensation in the operating range we are interested with the considered stack of materials.

As expected from the simulation, filling the sensing cavity with a periodic grating synchronous with the IDT and mirror periodicity prevents acoustic modes from being confined in the cavity. These two cases – empty cavity and patterned cavity – are presented in Fig. 18 (blue and magenta for the patterned cavity, red and green for the empty cavity). In both cases the temperature sensitivity is significant and representative of the thermal behavior of the underlying ST-cut quartz substrate with a -35 ppm/K first order temperature coefficient of frequency (TCF_1). Notice the gradual increased acoustic losses as temperature rises. Patterning the same resonator (Fig. 19) with different guiding layer thicknesses allows for an estimate of the gravimetric sensitivity: as found in the case of delay lines, the resonators exhibit gravimetric sensitivities in the **350 cm^2/g** range. Hence, the disappointing conclusion in terms of sensitivity, which was already hinted at by the delay line analysis, is that modelling expects excessive gravimetric sensitivities due to unachievable narrow operating conditions, and practical observations are in the same range of sensitivities as those found for optimal layer thicknesses of silicon dioxide guiding layers. The manufacturing process is however significantly simplified when using polymeric, photosensitive guiding layers rather than silicon dioxide. Furthermore, a given quartz substrate patterned

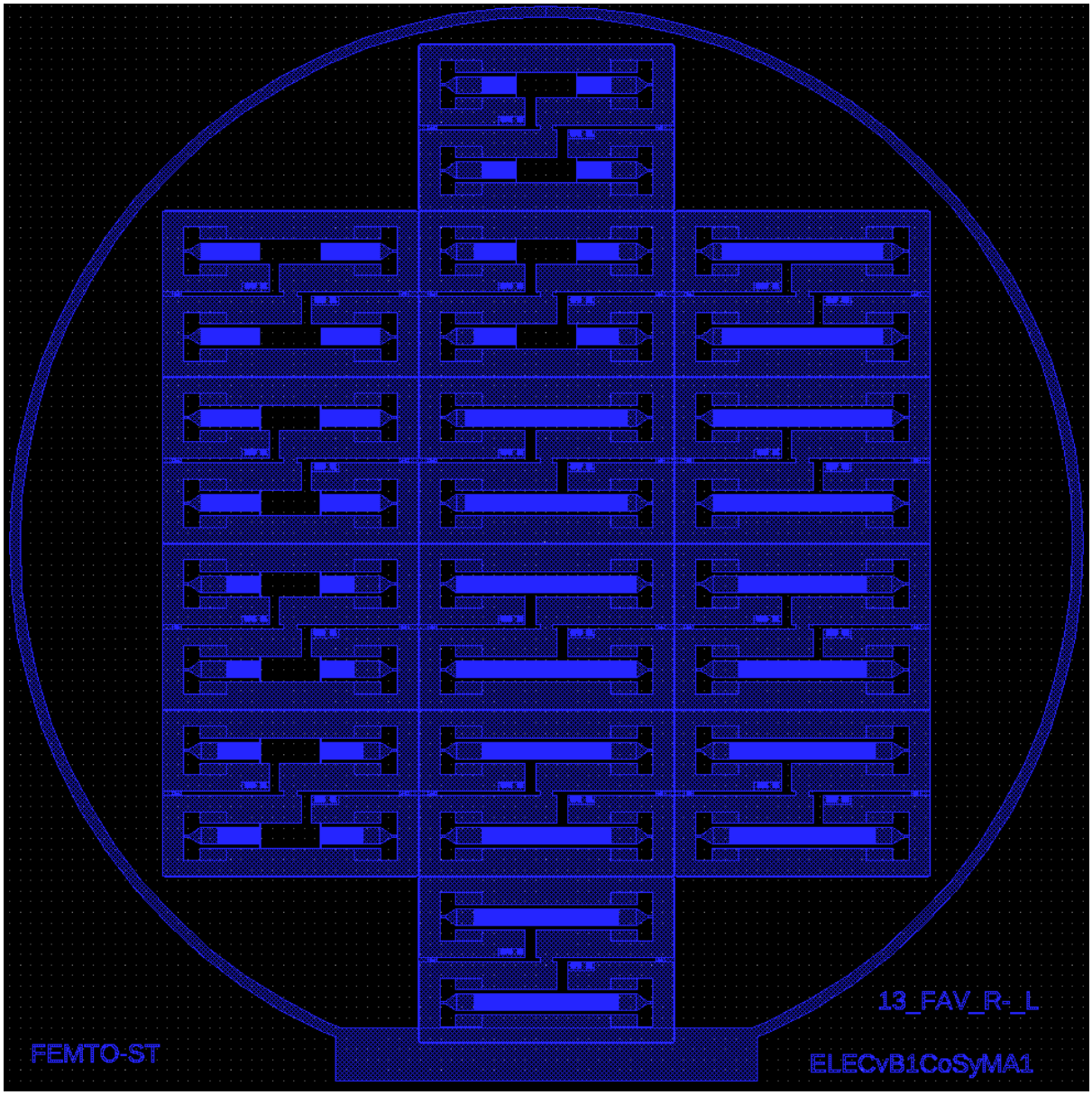

Figure 17: Mask layout for prototyping the various acoustic resonator configurations discussed in the text.

with electrodes is usable multiple times by stripping the photoresist using an organic solvent and coating a new guiding layer.

Beyond the gravimetric sensitivity, two additional parameters significantly define the detection limit of the whole instrument including the transducer and the associated instrumentation: temperature drift sensitivity and phase to frequency slope.

The latter parameter is experimentally characterized for all resonator and delay line configurations at temperatures ranging from ambient to 70^{o}C. As can be seen on Fig. 20, the classical AT cut which usually exhibits a turnover temperature around ambient now exhibits the strongest sensitivity to temperature due to the additional guiding layer influence. On the other hand, the temperature drift of the ST cut quartz has been significantly reduced by the guiding layer: an optimum photoresist thickness would allow for a tradeoff between maximizing the gravimetric sensitivity (thickness in the 1.2 μm range at 155 MHz) and reducing the temperature sensitivity (thickness in the 1.0 μm range at 155 MHz).

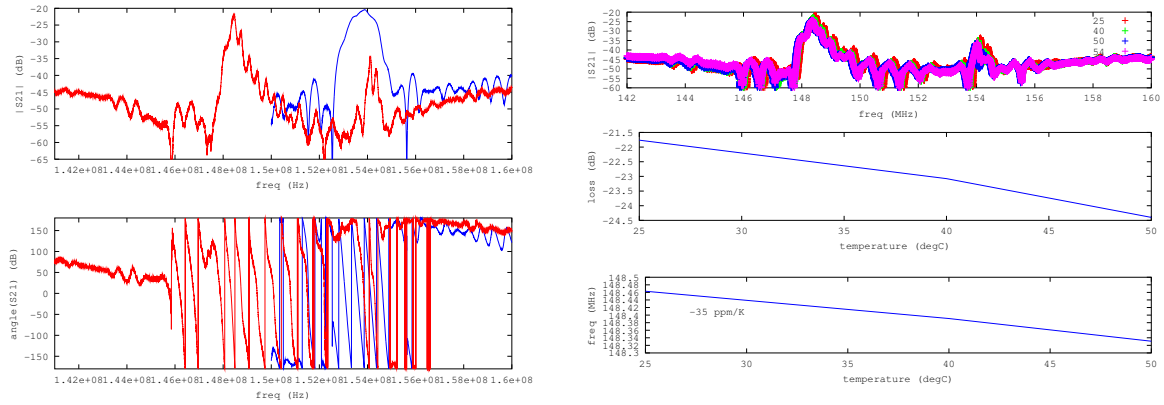

Figure 18: Left: comparison of the resonator and delay line transfer functions. Right: temperature dependence of the resonator transfer function – losses (magnitude) and acoustic velocity (1250 nm thick S1813 photoresist over 600 nm Al electrodes), yielding a -35 ppm/K value for the latter parameter.

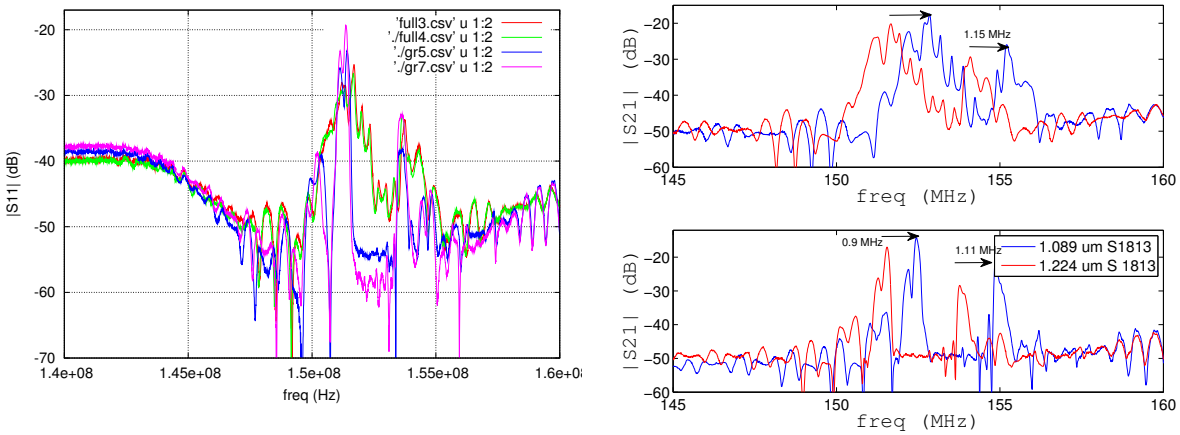

Figure 19: Left: comparison of the two resonator designs including or lacking periodically patterned electrodes in the sensing cavity. Notice how the grating, as expected from the simulations, prevents the acoustic modes from being confined in the cavity and lower the insertion losses and the stop band input. Right: gravimetric sensitivity assessment observed by coating the same 440 nm-thick aluminum electrode patterns on ST-cut quartz with two different S1813 photoresist thicknesses (1220 and 1090 nm).

The second parameter is the slope of the phase to frequency relationship. Indeed, since our openloop electronics measures a phase, the steeper the slope, the better the ability to detect minute frequency variations. The resonators (Fig. 20, right) exhibit a steep slope of -1910 deg/MHz (resonator on ST-cut quartz coated with 1089 nm S1813 photoresist) to -1760 deg/MHz (resonator on ST-cut quartz coated with 1224 nm S1813 photoresist). The delay line, with no targeted acoustic wave confinement, is observed to exhibit a phase to frequency slope of -675 deg/MHz. This value compares favorably with the predicted slope of

$$\frac{d\varphi}{df} = 360 \times \frac{L}{\lambda f}$$

with $L = 9$ mm the acoustic path length, $f \simeq 155$ MHz the operating frequency, $\lambda = 32$ μ the acoustic wavelength yielding a slope value of 650 deg/MHz.

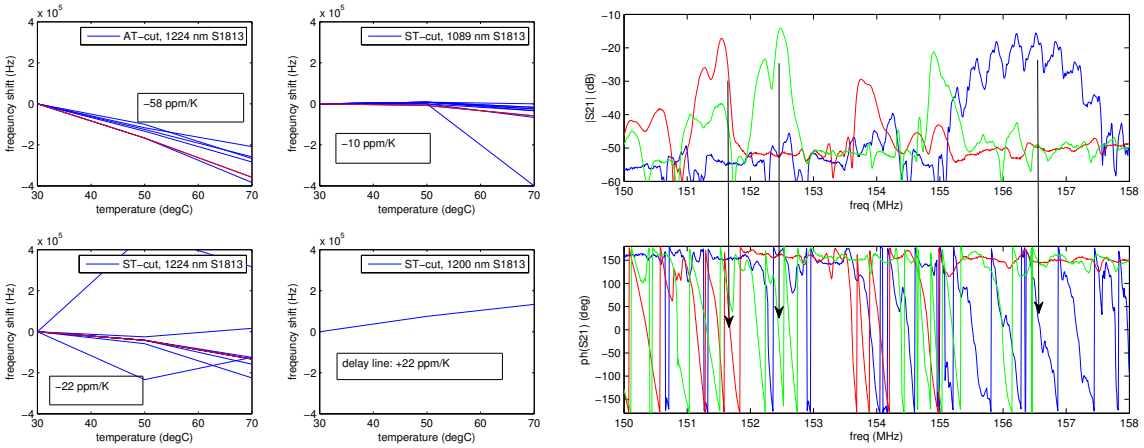

Figure 20: Left: temperature sensitivity of ST and AT-cut transducers, all resonator configurations (top and bottom left) and delay line configuration (bottom right). Right: phase to frequency slope identification close to the transfer maximum frequency. Notice the ripples in the band pass of the delay line, due to the sharp dicing of the chip: such artifacts would disappear once the sensor is packaged and surrounded by an acoustic absorber preventing reflections of the acoustic wave on the sides of the chip.

7 Conclusion

Having implemented the basic elements for modelling the behavior of a Love mode acoustic transducer confining the acoustic wave in a PMMA layer, we have identified appropriate operating points for designing a resonator configuration. Two conditions concerning the acoustic cavity – patterned with a grating synchronous with the IDT and mirrors, or free of electrodes – allow for selecting whether modes confined in the cavity are allowed or not. In the latter case, the spectra are clearly identified with only two acoustic modes at the stop band input and output, while otherwise additional modes are present between these two frequencies. Such conditions are confirmed experimentally.

However, the acoustic losses in the case of resonators does not exhibit improvement with respect to the delay line approach, nor does the gravimetric sensitivity. The selection between acoustic delay line and resonator is then confined to the selection of the phase v.s frequency slope, whose steepness is increased 3-fold in the latter case with respect to the former. Whether the resolution advantage balances the increased sensor dimension remains to be discussed.

Multiple perspectives concerning the simulations remain to be explored:

- effect of the conformal shape of the guiding layer over the electrodes, especially since the transfer of the electrode shape to the resist surface is questionable following our topography measurements,
- effect of the shape of the region of the polymer over the electrode (replace a rectangle with a trapezoid representative of the effect of surface tension forces when spin coating the photoresist
- introduce the effect of viscous water over the sensing cavity.

Furthermore, the conclusion about the different dependence with temperature of ST-cut delay lines and resonators deserves additional investigation since this result is rather unexpected. Practical use of the resonators fitted with fluidic cells remains to be demonstrated.

References

[1] D. Royer, E. Dieulesaint, D.P. Morgan, *Elastic Waves in Solids I: Free and Guided Propagation (Advanced Texts in Physics)*, Springer (2000)

[2] J.-M. Friedt, L. Francis, K.-H. Choi, and A. Campitelli, *Combined Atomic Force Microscope and Acoustic Wave Devices: Application to Electrodeposition*, J. Vac. Sci. Tech. A **21** (4), pp.1500- (2003)

[3] W.W Ang, H. Oh, K. Lee, S. Yang, *Enhanced Sensitivity of Wireless Chemical Sensor Based on Love Wave Mode*, Japanese Journal of Applied Physics **47** (9), pp. 7372–7379 (2008)

[4] Song, Taehyeon; Song, Seung Yeon; Yoon, Hyun C.; Lee, Keekeun, *Development of a Wireless Love Wave Biosensor Platform for Multi-functional Detection*, Japanese Journal of Applied Physics **50** (6), pp. 06GL09-06GL09-6 (2011) referenced at `http://adsabs.harvard.edu/abs/2011JaJAP..50fGL09S`

[5] H. Oh, W. Wang, K. Lee, H.C. Yoon, S. Yang, *Wirelessly Driven and Battery-Free Love Wave Biosensor Based on Dinitrophenyl Immobilization*, Japanese Journal of Applied Physics **48** pp.06FJ05 (2009)

[6] J.-M. Friedt, S. Alzuaga, N. Ratier, N. Vercelloni, R. Boudot, B. Guichardaz, W. Daniau, V. Laude, S. Ballandras, *Design of Asynchronous STW Resonators for Filters and High Stability Source Applications*, 2005 IEEE International Ultrasonics Symposium (UFFC), Rotterdam, The Netherlands (18-21 September 2005)